Wideband enhancement of infrared absorption in a direct band-gap semiconductor by using nonabsorptive pyramids

Citation: Dai, Weitao, Daniel Yap, and Gang Chen. "Wideband Enhancement of Infrared Absorption in a Direct Band-gap Semiconductor by Using Nonabsorptive Pyramids." Optics Express 20.S4 (2012): A519. © 2012 OSA

As Published: http://dx.doi.org/10.1364/OE.20.00A519

Publisher: Optical Society of America

Persistent URL: http://hdl.handle.net/1721.1/78279

Version: Final published version: final published article, as it appeared in a journal, conference proceedings, or other formally published context

Wideband enhancement of infrared absorption in a direct band-gap semiconductor by using nonabsorptive pyramids

Weitao Dai,[1] Daniel Yap,[2] and Gang Chen[1,*]

[1]*Department of Mechanical Engineering, Massachusetts Institute of Technology, 77 Massachusetts Avenue, Cambridge, Massachusetts 02139, USA*
[2]*HRL Laboratories, LLC. 3011 Malibu Canyon Road, Malibu, California 90265, USA*
[*]*gchen2@mit.edu*

Abstract: Efficient trapping of the light in a photon absorber or a photodetector can improve its performance and reduce its cost. In this paper we investigate two designs for light-trapping in application to infrared absorption. Our numerical simulations demonstrate that nonabsorptive pyramids either located on top of an absorbing film or having embedded absorbing rods can efficiently enhance the absorption in the absorbing material. A spectrally averaged absorptance of 83% is achieved compared to an average absorptance of 28% for the optimized multilayer structure that has the same amount of absorbing material. This enhancement is explained by the coupled-mode theory. Similar designs can also be applied to solar cells.

OCIS codes: (040.0040) Detectors; (350.4238) Nanophotonics and photonic crystals.

References and links

1. E. A. Alsema, "Energy pay-back time and CO_2 emissions of PV systems," Prog. Photovoltaics **8**, 17–25 (2000).
2. K. Taretto and U. Rau, "Modeling extremely thin absorber solar cells for optimized design," Prog. Photovoltaics **12**, 573–591 (2004).
3. H. Deckman, C. Roxlo, and E. Yablonovitch, "Maximum statistical increase of optical-absorption in textured semiconductor-films," Opt. Lett. **8**, 491–493 (1983).
4. P. Sheng, A. Bloch, and R. Stepleman, "Wavelength-selective absorption enhancement in thin-film solar-cells," Appl. Phys. Lett. **43**, 579–581 (1983).
5. C. Heine and R. H. Morf, "Submicrometer gratings for solar energy applications," Appl. Opt. **34**, 2476–2482 (1995).
6. H. A. Atwater and A. Polman, "Plasmonics for improved photovoltaic devices," Nat. Mater. **9**, 205–213 (2010).
7. L. Hu, X. Chen, and G. Chen, "Surface-plasmon enhanced near-bandgap light absorption in silicon photovoltaics," J. Comput. Theor. Nanosci. **5**, 2096–2101 (2008).
8. L. Hu and G. Chen, "Analysis of optical absorption in silicon nanowire arrays for photovoltaic applications," Nano Lett. **7**, 3249–3252 (2007).
9. S. E. Han and G. Chen, "Optical absorption enhancement in silicon nanohole arrays for solar photovoltaics," Nano Lett. **10**, 1012–1015 (2010).
10. S. E. Han and G. Chen, "Toward the Lambertian limit of light trapping in thin nanostructured silicon solar cells," Nano Lett. **10**, 4692–4696 (2010).
11. J. Zhu, Z. Yu, G. F. Burkhard, C.-M. Hsu, S. T. Connor, Y. Xu, Q. Wang, M. McGehee, S. Fan, and Y. Cui, "Optical Absorption enhancement in amorphous silicon nanowire and nanocone arrays," Nano Lett. **9**, 279–282 (2009).

#165787 - $15.00 USD Received 30 Mar 2012; revised 25 May 2012; accepted 25 May 2012; published 15 Jun 2012

12. M. D. Kelzenberg, S. W. Boettcher, J. A. Petykiewicz, D. B. Turner-Evans, M. C. Putnam, E. L. Warren, J. M. Spurgeon, R. M. Briggs, N. S. Lewis, and H. A. Atwater, "Enhanced absorption and carrier collection in Si wire arrays for photovoltaic applications," Nat. Mater. **9**, 239–244 (2010).
13. G. Gomard, E. Drouard, X. Letartre, X. Meng, A. Kaminski, A. Fave, M. Lemiti, E. Garcia-Caurel, and C. Seassal, "Two-dimensional photonic crystal for absorption enhancement in hydrogenated amorphous silicon thin film solar cells," J. Appl. Phys. **108**, 123102 (2010).
14. B. E. A. Saleh and M. C. Teich, *Fundamentals of Photonics*, 2nd ed. (Wiley, 2007).
15. G. J. Bauhuis, P. Mulder, E. J. Haverkamp, J. C. C. M. Huijben, and J. J. Schermer, "26.1% thin-film GaAs solar cell using epitaxial lift-off," Sol. Energy Mater. Sol. Cells **93**, 1488–1491 (2009).
16. P. Yu, C.-H. Chang, C.-H. Chiu, C.-S. Yang, J.-C. Yu, H.-C. Kuo, S.-H. Hsu, and Y.-C. Chang, "Efficiency enhancement of GaAs photovoltaics employing antireflective indium tin oxide nanocolumns," Adv. Mater. **21**, 1618–1621 (2009).
17. L.-K. Yeh, K.-Y. Lai, G.-J. Lin, P.-H. Fu, H.-C. Chang, C.-A. Lin, and J.-H. He, "Giant efficiency enhancement of GaAs solar cells with graded antireflection layers based on syringelike ZnO nanorod arrays," Adv. Energy Mater. **1**, 506–510 (2011).
18. K.-S. Han, J.-H. Shin, W.-Y. Yoon, and H. Lee, "Enhanced performance of solar cells with anti-reflection layer fabricated by nano-imprint lithography," Sol. Energy Mater. Sol. Cells **95**, 288–291 (2011).
19. A. Taflove and S. Hagness, *Computational Electrodynamics: the Finite-Difference Time-Domain Method* (Artech, 2000).
20. A. F. Oskooi, D. Roundy, M. Ibanescu, P. Bermel, J. D. Joannopoulos, and S. G. Johnson, "MEEP: a flexible free-software package for electromagnetic simulations by the FDTD method," Comput. Phys. Commun. **181**, 687–702 (2010).
21. E. D. Palik, *Handbook of Optical Constants of Solids* (Academic, 1985).
22. P. Campbell and M. A. Green, "Light trapping properties of pyramidally textured surfaces," J. Appl. Phys. **62**, 243–249 (1987).
23. A. K. Dutta, R. Olah, G. Mizuno, R. Sengupta, J. H. Park, P. Wijewarnasuriya, and N. Dhar, "High efficiency solar cells based on micro-nano scale structures," Proc. SPIE **7683**, 768300 (2010)
24. J. Zhu, C.-M. Hsu, Z. Yu, S. Fan, and Y. Cui, "Nanodome solar cells with efficient light management and self-cleaning," Nano Lett. **10**, 1979–1984 (2010).
25. R. Esteban, M. Laroche, and J. J. Greffet, "Dielectric gratings for wide-angle, broadband absorption by thin film photovoltaic cells," Appl. Phys. Lett. **97**, 221111 (2010).
26. B. M. Kayes, H. A. Atwater, and N. S. Lewis, "Comparison of the device physics principles of planar and radial p-n junction nanorod solar cells," J. Appl. Phys. **97**, 114302 (2005).
27. H. A. Haus, *Waves and Fields in Optoelectronics* (Prentice Hall, 1984).
28. S. Fan, W. Suh, and J. D. Joannopoulos, "Temporal coupled-mode theory for the Fano resonance in optical resonators," J. Opt. Soc. Am. A **20**, 569–572 (2003).
29. Z. Yu, A. Raman, and S. Fan, "Fundamental limit of nanophotonic light trapping in solar cells," Proc. Natl. Acad. Sci. USA **107**, 17491–17496 (2010).
30. Z. Yu, A. Raman, and S. Fan, "Fundamental limit of light trapping in grating structures," Opt. Express **18**, A366–A380 (2010).
31. C. Kittel, *Introduction to Solid State Physics*, 7th ed. (Wiley, 1995).
32. M. Deubel1, G. von Freymann1, M. Wegener, S. Pereira, K. Busch, and C. M. Soukoulis, "Direct laser writing of three-dimensional photonic-crystal templates for telecommunications," Nat. Mater. **3**, 444–447 (2004).
33. E. Kim, Y. Xia, and G. M. Whitesides, "Polymer microstructures formed by moulding in capillaries," Nature **376**, 581–584 (2002).

Light-trapping is essential for solar cells and photodetectors. For solar cells, light-trapping reduces the required amount of the photovoltaic materials, which brings down the cost [1] and improves carrier collection [2]. Much effort has been devoted into designing effective light-trapping structures for solar cells. Some general design strategies include anti-reflection structures at the top, random [3] or periodic [4–6] structures at the surfaces of the absorbing material to scatter light, highly localized fields excited using surface plasmons [6, 7], and formation of the absorbing material into nanostructures [8–13]. For thin-film semiconductor photodetectors, a reduction of the volume of absorbing material that is enabled by light trapping also serves to improve the signal to noise ratio [14]. Compared to intensive research of light trapping in silicon photovoltaic cells, for which the material absorption can be quite low, less research has been devoted to broadband light-trapping in photodetectors or photovoltaic cells that have direct-bandgap absorbing material [15–18].

#165787 - $15.00 USD Received 30 Mar 2012; revised 25 May 2012; accepted 25 May 2012; published 15 Jun 2012

In this paper we report on our investigation of light-trapping structures for infrared photodetectors working in the wavelength range from 1μm to 5μm. Simulations were performed with the finite-difference time-domain (FDTD) method [19], using a freely available software package [20]. Given the objects' geometries in the simulation area and their material properties, the simulation software package uses Maxwell's equations and determines the electric and magnetic field distributions. Absorption spectra and other electromagnetic variables can be further calculated based on these field distributions. The absorption of light by a material can be determined from the imaginary part of the permittivity of the material. The relative permittivity ε_a of the active material in our structure is described by the summation of Lorentzian functions:

$$\varepsilon_a = \varepsilon_\infty + \sum_m \frac{\omega_{p,m}^2}{\omega_{0,m}^2 - \omega^2 - i\omega\gamma_m}. \quad (1)$$

Here $\omega = 2\pi c/\lambda$ (c is the speed of light in vacuum and λ is the wavelength in vacuum). The parameters in Eq. (1) are $m = 2$, $\varepsilon_\infty = 7.14$, $\omega_{0,1} = 2.29$PHz, $\omega_{p,1} = 5.11$PHz, $\gamma_1 = 128$PHz,$\omega_{0,2} = 7.53$PHz, $\omega_{p,2} = 16.8$PHz, $\gamma_2 = 4.63$PHz, 1PHz $= 10^{15}$Hz. The refractive index of the active material is $n_a = \sqrt{\varepsilon_a}$. The real part of the refractive index is around 3.5 and the imaginary part is around 0.1. InAs has similar refractive index values [21]. Since in this work we are focusing on the "improvement" of the absorption, the precise refractive index values are not important. The effective thickness d_{eff} used as a parameter of a light-trapping structure in this work is defined as the thickness of a uniform-thickness film which contains the same amount of absorbing material as found in the light-trapping structure. Our goal is an absorber structure whose effective thickness is much smaller than the wavelength.

The first proposed light-trapping design is a nonabsorptive pyramid array on top of an active film, which is shown in Fig. 1(a). A surface textured with pyramids has been demonstrated to have enhanced trapping of the incident light [10, 22–24]. It functions as a broadband antireflection layer and also scatters light efficiently to increase the optical path length in the active material. In our design, the light-absorbing layer is quite thin and thus we use another nonabsorptive material to form the pyramids. Similar ideas were presented previously for photovoltaic cells having a one-dimensional grating located above a thin active layer [25]. Since the photodetectors we investigated are intended to work in the infrared regime, silicon will be a good choice for the nonabsorptive pyramids. Its refractive index is close to the real part of the refractive index of the active material, which minimizes the reflection at the interfaces between the nonabsorptive pyramid and the regions of active material. The pyramids are arranged in a square lattice with a lattice constant $a = 3\mu$m. The pyramid has a square base with width $w = 3\mu$m and height $h = 6\mu$m. Under the pyramid layer is the 0.3μm-thick active layer with a 0.4μm-thick SiO_2 layer and a gold reflector in the backside. The refractive index of silicon is set as 3.5 in the simulations.

The absorption spectrum of this structure under normal incidence is compared in Fig. 1(c) with the absorption spectrum of an optimized multilayer structure. The multilayer structure consists of, from top to bottom, a 1.5μm-thick SiO_2 layer, a 0.3μm-thick active layer, a 20nm-thick SiO_2 layer and a gold reflector. The thicknesses of the two SiO_2 layers are optimized to achieve the highest value, which is 0.28, for its absorptance averaged over the $1-5\mu$m wavelength range. In comparison, the pyramid structure achieves a spectrally averaged absorptance of 0.69. Furthermore, we can achieve even higher absorption by embedding absorptive nanorods within otherwise nonabsorptive pyramids. The active nanorods in the pyramids shown in Fig. 1(b) have a height of $h_{rod} = 6.3\mu$m, radius $r_{rod} = 0.4\mu$m and $d_{eff} = 0.3\mu$m. The nonabsorptive pyramid structure includes the pyramids and a 0.3μm-thick spacer layer. The average absorptance for this nanorods structure is 0.79.

Nanorod arrays have been studied extensively as a light-trapping scheme [8, 9, 12]. Nanorods

#165787 - $15.00 USD Received 30 Mar 2012; revised 25 May 2012; accepted 25 May 2012; published 15 Jun 2012

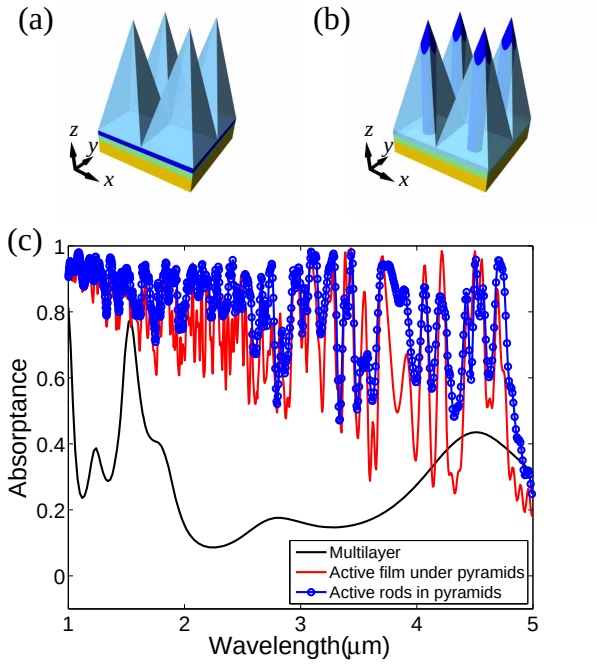

Fig. 1. (a) Light trapping structure with an active film under nonabsorptive pyramids. From top to bottom: the nonabsorptive pyramids (transparent light blue), the active film (blue, 0.3μm thick), the SiO_2, layer (green, 0.4μm thick) and the gold reflector (golden). The pyramids have lattice constant $a = 3\mu$m and pyramid height $h = 6\mu$m. (b) Light-trapping structure with active rods embedded in nonabsorptive pyramids. The rods have the height $h_{rod} = 6.3\mu$m, radius $r_{rod} = 0.4\mu$m and effective thickness $d_{eff} = 0.3\mu$m. (c) The absorption spectra of the two light-trapping structures illustrated in (a) and (b) along with the absorption spectrum of an optimized multilayer structure. The multilayer structure consists of, from top to bottom, a 1.5μm-thick SiO_2 layer, a 0.3μm-thick active layer, a 20nm-thick SiO_2 layer and a gold reflector.

with radial p-n junctions may simultaneously provide long optical path lengths and short carrier collection lengths [26]. Our simulations show that the addition of nonabsorptive pyramids, into which the nanorods are embedded, will improve the absorption in the nanorods even further. Figure 2 compares the absorption spectra of the nanorods with and without the pyramids. The average absorptance drops from 0.79 to 0.58 when the nonabsorptive pyramids are removed. In Fig. 3, we plot the reflection spectra from the front surface of the active rod structure with or without nonabsorptive pyramids. Both structures exhibit excellent broadband antireflection properties. Though less reflection from the front surface is an important reason for the absorption enhancement over the multilayer structure shown in Fig. 1(c), we cannot use it to explain the absorption difference shown in Fig. 2. To explain this difference in absorption, we have to consider the interaction between the incident electromagnetic wave and these three dimensional structures. Coupled-mode theory [27, 28] allows us to characterize a complex optical system in the wave optics regime using just a few parameters.

The coupled-mode theory describes the interactions between the incident light and the structure as the excitation and extinction of resonant modes within the structure. The absorption

#165787 - $15.00 USD Received 30 Mar 2012; revised 25 May 2012; accepted 25 May 2012; published 15 Jun 2012

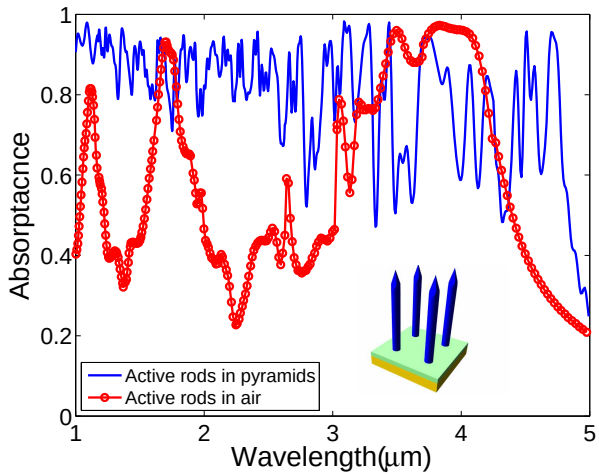

Fig. 2. Absorption spectra of active rod structures with nonabsorptive pyramids, as shown in Fig. 1(b), and without the nonabsorptive pyramids. The inset shows an illustration of structure with the active rods in air, without any nonabsorptive pyramids

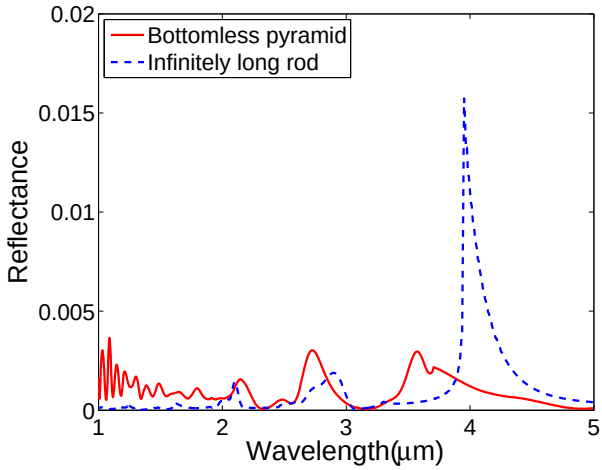

Fig. 3. Reflectance spectra of the bottomless pyramid structure and the infinitely long rod structure. The bottomless pyramid structure has the same parameters as the structure shown in Fig. 1(b) except the nonabsorptive pyramids and the active rods extend to infinity in the $-z$ direction. The infinitely long rod structure is a bottomless pyramid structure for which the nonabsorptive pyramids are replaced by air.

#165787 - $15.00 USD Received 30 Mar 2012; revised 25 May 2012; accepted 25 May 2012; published 15 Jun 2012

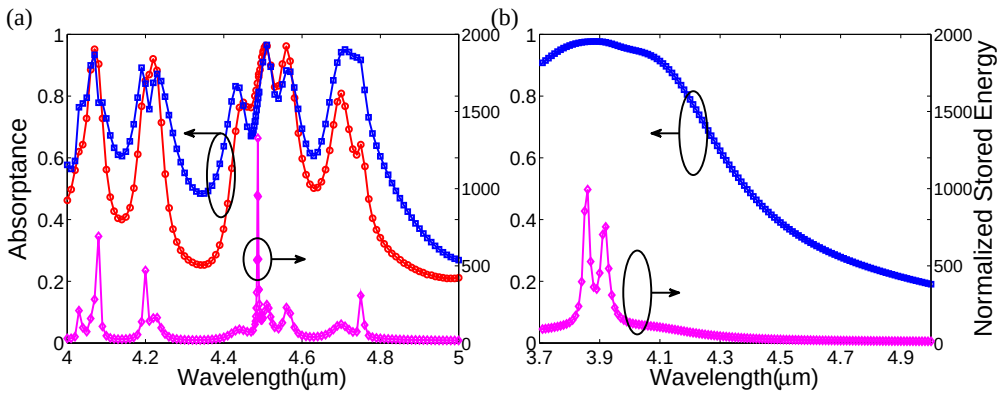

Fig. 4. (a) Absorption spectra of the light-trapping structures shown in Fig. 1(a) (red curve with circles) and 1(b) (blue curve with squares), along with the spectral distribution of the energy stored in a pyramid structure that doesn't have any active material. The stored energy is normalized by the electromagnetic energy carried by the incident plane wave in the same volume of free space. (b) Absorption spectrum of the light-trapping structures shown as the inset of Fig. 2, along with the spectral distribution of normalized energy stored in that rod structure when the rod is lossless.

spectrum contributed by one resonant mode is [29, 30]

$$A(\omega) = \frac{\gamma_i \gamma_{e,0}}{(\omega - \omega_0)^2 + (\gamma_i + \sum_m \gamma_{e,m})^2/4}. \tag{2}$$

Here ω_0 is the resonant frequency. γ_i and $\gamma_{e,m}$ describe how energy leaves the excited mode: γ_i is internal energy loss rate through absorption by the active material within the structure and $\gamma_{e,m}$ is the external energy loss rate from having the light coupled out of the structure. This light is seen as being reflected or back-scattered by the structure. The subscript m means there are several out-coupling channels. $\gamma_{e,0}$ (with $m = 0$) also describes the energy injection or in-coupling rate from the incident light into that resonant mode. The absorption spectrum has a peak at the resonance wavelength of the mode. Many modes exist in this structure. Therefore, the final absorption spectrum is the summation of the contributions from each of those modes. Generally speaking, more excited modes results in higher spectrum-integrated absorption. Higher refractive index materials support more modes. For example the density of states is proportional to n^3 for bulk materials [31]. So replacing air with silicon will increase the number of modes significantly. We can see in Fig. 2 that the absorption spectrum of the structure with active rods in high-index pyramids has many more peaks than the spectrum of the structure with active rods in air.

Another important feather of Fig. 1(c) is that the peaks of the absorption spectra of the two structures shown in Fig. 1(a) and 1(b) are always located at the same wavelengths. Figure 4(a) plots the details of the two spectra for the wavelengths between 4μm and 5μm along with the energy stored in a pyramid structure of the same dimensions that does not contain any active material. Based on the coupled-mode theory, the energy stored in a mode of the passive structure is

$$\text{Energy} \propto \frac{\gamma_{e,0}}{(\omega - \omega_0)^2 + (\sum_m \gamma_{e,m})^2/4}. \tag{3}$$

$\gamma_i = 0$ here because no absorbing material exists. If we can assume that $\gamma_{e,m}$ is not affected significantly by the presence and locations of the absorbing material in the pyramidal structure, the stored energy spectrum should have the same peak wavelengths and have narrower peak

#165787 - $15.00 USD Received 30 Mar 2012; revised 25 May 2012; accepted 25 May 2012; published 15 Jun 2012

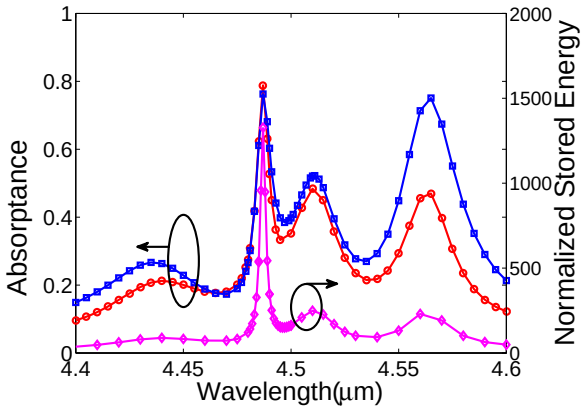

Fig. 5. Absorption spectra of a low loss pyramid structure (red curve with circles) and a structure with low loss absorbing rods embedded in nonabsorptive pyramids (blue curve with squares), along with the spectral distribution of the energy stored in a pyramid structure that doesn't have any active material. The permittivity of the active material in the low loss pyramid structure is $12.25+0.01i$; the permittivity of the active material in the low loss rod structure is $12.25+0.1i$. Originally the permittivity of the active material is around $12.2+0.65i$.

widths compared with the absorption spectra. The simulation results shown in Fig. 4(a) indeed confirm this behavior. A similar analysis was done for the structure with active rods in air (without the nonabsorptive pyramids) and the results are shown in Fig. 4(b). Obviously the two closely spaced modes with resonant wavelength near 3.9μm are responsible for the broad absorption peak around 3.9μm. These results show that the many resonant modes supported by the high-index pyramids do improve the spectrally integrated absorption that occurs in the small active volume of the light-trapping pyramidal structures.

The only anomaly is the very high peak at 4.49μm evident in the stored energy spectrum shown in Fig. 4(a). Note that the absorption spectra do not show a corresponding peak at this wavelength. This peak in the stored energy spectrum is very narrow, which suggests that for the associated mode, $\sum_m \gamma_{e,m}$ are small based on Eq. (3). In addition, if $\gamma_i \gg \sum_m \gamma_{e,m}$, the contribution from this mode to the absorption spectrum will be small based on Eq. (2). Note $\gamma_{e,0}$ is one of $\gamma_{e,m}$. When $\sum_m \gamma_{e,m}$ is small, $\gamma_{e,0}$ also is small. However, if the value for γ_i is even smaller, we can observe a distinct absorptive peak around 4.49μm. We show in Fig. 5 the absorptance spectrum obtained for a structure for which the whole pyramid is absorptive but the value for the imaginary part of the relative permittivity of the active material is only 0.01 compared to a value of 0.65 for the active material in the structure of Fig. 4(a). In this case, there is a pronounced peak at 4.49μm in the absorption spectrum. Likewise, Fig. 5 also shows the absorptance spectrum of a structure with an active but lower loss rod. The active material in that rod has a value of only 0.1 for the imaginary part of its relative permittivity. Again, the absorptance spectrum has a distinct peak at 4.49μm.

Additional insight can be provided by considering the optical-field distributions of the light in these structures. These field distributions are a superposition of the distributions for the different modes excited simultaneously in the structure. Figure 6 shows the electric-field energy density distributions obtained at the wavelength of 4.510μm for five different cases. In Fig. 6(a), the entire pyramid is lossless. In Fig. 6(b), the entire pyramid consists of a low loss active material. In Fig. 6(c), the structure has a low-loss active rod embedded in each otherwise transparent

#165787 - $15.00 USD Received 30 Mar 2012; revised 25 May 2012; accepted 25 May 2012; published 15 Jun 2012

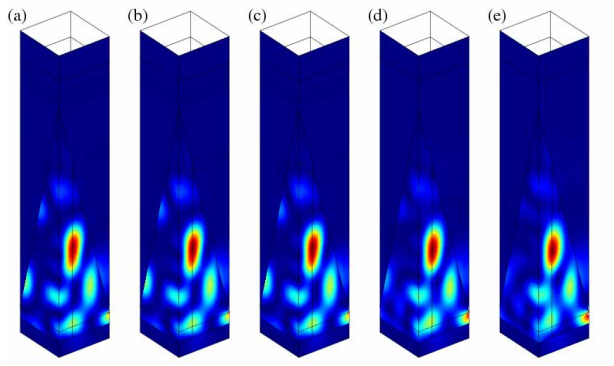

Fig. 6. Electric-field energy density distributions along two cross sections of a pyramid when the wavelength of the light is 4.510μm. (a) The entire pyramid is lossless; (b) The entire pyramids consists of a low loss material with $\varepsilon_a = 12.25 + 0.01i$; (c) The structure has a low loss active rod with $\varepsilon_a = 12.25 + 0.1i$ embedded in each otherwise transparent pyramid; (d) The structure has an active rod with $\varepsilon_a = 12.2 + 0.65i$ embedded in each otherwise transparent; (e) The structure has an active film with $\varepsilon_a = 12.2 + 0.65i$ under transparent pyramids. The maximum value for the electric-field energy density shown in each figure (dark red region) is (a) 3.7×10^{-9}J/m^3; (b) 2.4×10^{-9}J/m^3; (c) 2.3×10^{-9}J/m^3; (d) 6.0×10^{-10}J/m^3; (e) 5.5×10^{-10}J/m^3. The electric-field of the incident plane wave has a magnitude of 1V/m.

pyramid. In Fig. 6(d), the structure has a higher loss active rod embedded in that pyramid. And, in Fig. 6(e), the structure has a transparent pyramid and a thin film of the higher loss active material located underneath the pyramid. We can see that the optical field distributions are similar to each other for all of these cases, which suggests that the same mode is excited by the incident light at this wavelength, although the intensity of the mode is weaker when the absorption is strong. Incidentally, the absorption spectra in Fig. 4(a) and Fig. 5 all show distinct peaks at 4.51μm. Also, the stored energy spectrum has a weak and broad peak at this wavelength, which suggests that $\sum_m \gamma_{e,m}$, and likely $\gamma_{e,0}$, is fairly large for this mode. As the loss of the active regions in the structure increases, one would then expect the absorptance peak at 4.510μm to become higher and higher, as observed from a comparison of Fig. 4(a) and Fig. 5.

For comparison, Fig. 7 shows the electric-field energy density distributions obtained at the wavelength of 4.488μm for these same five cases. We can see that the optical field distributions are similar to each other for the first three of these cases, which again suggests that the same mode is excited by the incident light at this wavelength. However, in Fig. 7(d) and Fig. 7(e), the electric-field energy density distributions obtained for the structure containing the higher loss active material are quite different from the electric-field energy density distributions obtained for the lossless pyramid. Thus, other modes are dominant in these latter two cases. In the absorption spectra for these latter two cases, which are shown in Fig. 4(a), there is significant absorptance at 4.488μm. But the even greater absorption of the nearby absorption peak at 4.510μm dominates the spectrum. In contrast, for the cases with low-loss absorbing regions, whose absorption spectra are shown in Fig. 5, the peak at 4.488μm is distinct from the weaker peak at 4.510μm.

The discussions above illustrate that the presence of the active material in a structure, when that active material has the same real part of the refractive index as the material of the nonabsorptive pyramids, will not change the resonance wavelengths. However, it can influence the absorption rate γ_i of various modes. We can thus fine tune the absorption spectrum by changing

#165787 - $15.00 USD Received 30 Mar 2012; revised 25 May 2012; accepted 25 May 2012; published 15 Jun 2012

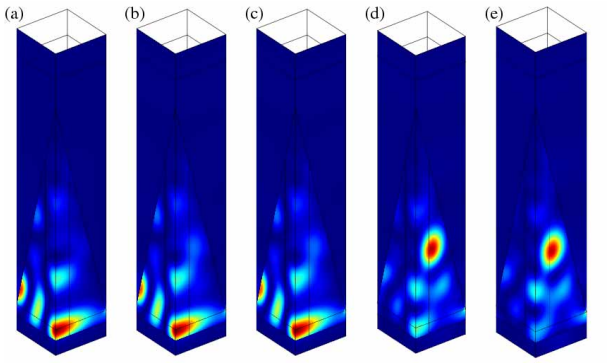

Fig. 7. Electric-field energy density distributions for the same five cases as Fig. 6 when the wavelength of the light is 4.488μm. The maximum value for the electric-field energy density in each figure is (a) 2.3×10^{-8}J/m^3; (b) 6.1×10^{-9}J/m^3; (c) 4.3×10^{-9}J/m^3; (d) 6.8×10^{-10}J/m^3; (e) 6.4×10^{-10}J/m^3.

the location and the shape of the active material. Such fine tuning is also evident when one compares the two absorption spectra shown in Fig. 4(a).

We now consider the effect of the shape and location of the active material on the value achieved for the spectrally averaged absorptance. Figure 8 shows the average absorptance of active rods within nonabsorptive pyramids when the height of the active rods h_{rod} changes from 6.3μm to 0.3μm. The radius of the rods changes with the height to keep $d_{eff}=0.3\mu$m. When $h_{rod}=0.3\mu$m, the rods become a thin film. The structure with rods $h_{rod}=4\mu$m has the maximum average absorptance 0.83. Generally speaking the average absorptance of a structure with pyramids remains high regardless of the shape of the active material within it, as compared with the average absorptance of a structure with absorbing rods that are not embedded in pyramids. The reason is because the nonabsorptive pyramids support many resonant modes in the broad wavelength range. There will always be some resonant modes which can contribute to the absorption spectrum significantly no matter where the active material is located.

The shape of the nonabsorptive pyramids will also influence the absorption. When the lattice constant is too small ($a<2\mu$m), the pyramids cannot scatter long wavelength light efficiently. So the absorption in the long wavelength regime becomes weak [10]. When the lattice constant changes from 3μm to 5μm with the pyramid height fixed at 6μm, our simulations show the average absorptance in the thin film structure remains the same and the average absorptance in the rod structure with $h_{rod}=6.3\mu$m decreases from 0.79 to 0.73. The main difference in their absorption characteristics appears in the short wavelength regime. In this regime we can treat the light as rays. When the lattice constant is larger, these rods become more sparsely distributed. More rays are reflected back without hitting the rods and the absorptance decreases. The pyramid height h also influences the absorption. The pyramids serve as a better anti-reflection layer when h increases. But the incremental improvement is small when $h>6\mu$m. In general, the nonabsorptive pyramids do enhance the absorption in the active material regardless of the specific shapes of those pyramids, although the values for the average absorptance obtained with each shape may be different.

Finding low-cost materials that have both a high refractive index and low loss in the visible regime is a significant challenge. If we want to extend the photodetectors' wavelength range into the visible regime or design similar structures for solar cells, we should also consider nonabsorptive pyramids that have a lower refractive index. Figure 9 shows how the absorption changes with the refractive index of the pyramids n_p. When the active material is a thin film,

#165787 - $15.00 USD Received 30 Mar 2012; revised 25 May 2012; accepted 25 May 2012; published 15 Jun 2012

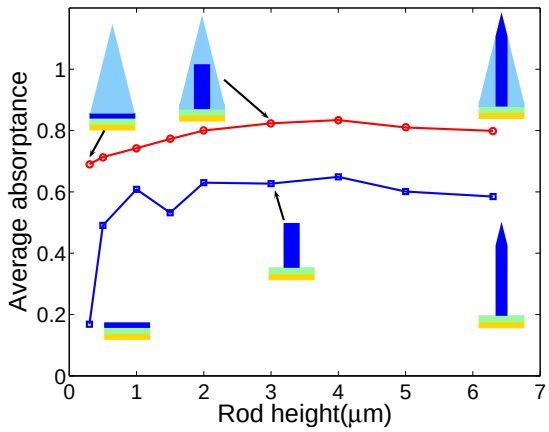

Fig. 8. Average absorptance for the wavelength range from 1μm to 5μm *vs.* the height of the active rods in the nonabsorptive pyramids. The red line with circles shows the average absorptance of active rods within nonabsorptive pyramids having $n_p = 3.5$. The blue line with squares shows active rods in air. The six insets show the cross section illustration of structures with or without the nonabsorptive pyramids, for values of $h_{rod} = 0.3\mu$m, 3μm or 6.3μm All of the structures have the same effective thickness $d_{eff} = 0.3\mu$m. Note that when $h_{rod} = 0.3\mu$m, the rod becomes a laterally continuous film.

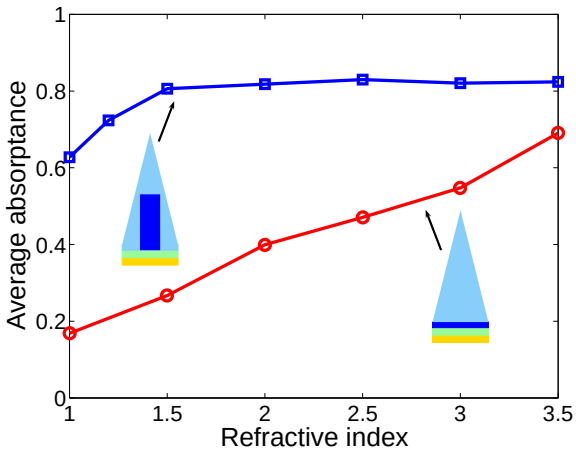

Fig. 9. Average absorptance for the wavelength range from 1μm to 5μm *vs.* the refractive index of the nonabsorptive pyramids. The red curve with circles represents the absorption in the structure having a 0.3μm-thick film; the blue curve with squares represents the absorption in the structure having active rods with $h_{rod} = 3\mu$m and $d_{eff} = 0.3\mu$m.

#165787 - $15.00 USD Received 30 Mar 2012; revised 25 May 2012; accepted 25 May 2012; published 15 Jun 2012

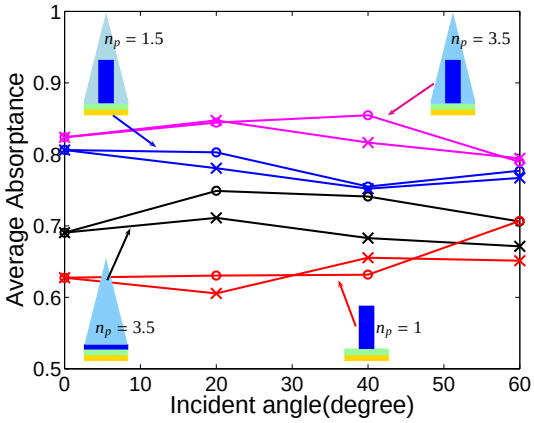

Fig. 10. Average absorptance for incident light in the wavelength range from 1μm to 5μm under oblique incidence angles. Four structures are studied that have: the 0.3μm-thick active film under the nonabsorptive pyramids with $n_p = 3.5$ (black); the active rods with $h_{rod} = 3\mu$m and $d_{eff} = 0.3\mu$m in the nonabsorptive pyramids with $n_p = 3.5$ (magenta), or with $n_p = 1.5$ (blue); and the same rods in air (red). The circles represent *s* polarization and the crosses represent *p* polarization.

the average absorptance increases almost linearly with an increase in n_p. But for the structures having active rods embedded in the pyramids with $h_{rod} = 3\mu$m, the average absorption increases quickly for small n_p and begins to saturate at a maximum value when n_p reaches 1.5. This means we have various choices of materials for constructing the transparent pyramids.

We also studied the angular and polarization dependence of the absorption. The results are shown in Fig. 10. Four designs were studied: a structure with a 0.3μm-thick active film under the nonabsorptive pyramids with $n_p = 3.5$; and structures with active rods with $h_{rod} = 3\mu$m and $d_{eff} = 0.3\mu$m in nonabsorptive pyramids whose refractive index is $n_p = 3.5$, $n_p = 1.5$ or $n_p = 1$. The incident plane is the $x-z$ plane shown in Fig. 1(a) and Fig. 1(b). Both *s* polarization and *p* polarization are simulated. At incidence angles up to 60°, the values for the average absorptance of all four designs remain high. Figure 10 shows clearly that the absorption is enhanced by the nonabsorptive pyramids for a large range of the incidence angles and for both polarizations of the light.

In the end of the paper we briefly address the pyramid fabrication. The nanorod rod array can be made by photolithography and etching, or other methods. If a polymer material is used to form the pyramids, we can fabricate these pyramids by depositing the polymer film and then use direct laser writing [32] or soft lithography techniques [18, 33] to define the pyramid shape. Depositing a high-index silicon or III-V semiconductor film on top of the nanorod array followed by some lithography method and etching can yield high-index pyramids.

In conclusion we presented two light-trapping designs: an active film under nonabsorptive pyramids and active rods embedded in nonabsorptive pyramids. Our simulations demonstrate the significant absorption enhancement provided by the nonabsorptive pyramids. We used coupled-mode theory to explain this enhancement. Although we design these structures for infrared photodetectors, similar design principles can also be used for solar cells.

Acknowledgments

This work was supported by DARPA and by a DoD MURI via UIUC.

#165787 - $15.00 USD Received 30 Mar 2012; revised 25 May 2012; accepted 25 May 2012; published 15 Jun 2012